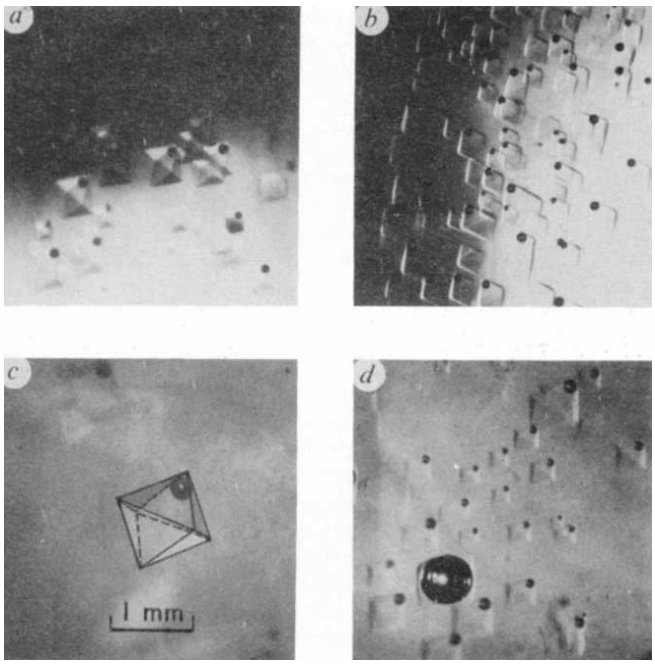

Fig. 1 Photographs of internal melt figures taken with a Polaroid camera. The scale of all the frames is drawn on frame *c*. All the melt figures are octahedra, and the larger octahedron in frame *c* is outlined in ink to help it to be easily seen. The small circular bubbles are the vapour spaces and the large bubble in frame *d* is on the surface of the clathrate and in the melt.

octahedra. This is as expected because tetrahydrofuran clathrate hydrate forms a cubic crystal and the octahedral planes are densely packed and so have a low energy[2]. Typically, the edges of the octahedra were about 0.1–1 mm long. The bubbles seemed to be very nearly spherical, which is not surprising because of the high surface tension and the small size. The diameter of typical bubbles made in this work was about 20–200 μm.

The bubbles occur in the melt figures because the liquid is denser than the clathrate and so leaves a space filled with water vapour and tetrahydrofuran vapour. The ratio of the volume of the bubble, assuming it is spherical, to the volume of the melt figure is $\pi(d/l)^3$, where d is the diameter of the bubble and l the length of the diagonals of the octahedron. The dimensions of several octahedra and their bubbles were measured on several-fold enlargements of Fig. 1 and the average ratio of the volume of the bubble to the volume of the octahedron was 0.018 ± 0.004. The melt is, therefore, denser than the clathrate by this fraction, which agrees with Gough and Davidson's[3] value of -0.01470 ± 0.00034.

Several pairs of octahedra grew together, as is seen in Fig. 1*a*. When they did so, the bubble in the lower figure rose to join the bubble in the upper.

All crystals that melt with a decrease of volume should form internal melt figures if heat can be dumped directly into the interior without conducting it from the outside surfaces. They should occur in some other structure II clathrate hydrates such as those of 2,5-dihydrofuran[5], propylene oxide[6], chloroform[7], and others. They should also occur in the many other crystals whose melt is denser than the crystal, such as gallium, germanium, silicon, indium antimonide, sphalerite, and many others. It should be particularly easy to make the melt figures in gallium because it melts at 29.8 °C and the liquid is about 3% denser than the crystal. Heat could be dumped into the interior by passing an electric current, and the figures might be detected by X-ray shadowing.

The melting presumably originates at major imperfections in the crystals, and the figures may provide a way of studying these imperfections, and some preliminary experiments have detected imperfections in ice that were generated by fast neutrons and γ-rays[8]. The melt figures can, of course, be used for orienting crystals, as was suggested over 50 years ago for the figures in hexagonal ice[9].

Knight and Knight[10] have shown how to make 'negative' crystals in ice without any fluid in them. They drilled a narrow hole in a single crystal near the melting point, inserted a hypodermic needle, and evacuated through the needle. With enough patience and a good enough seal between the needle and an appropriate crystal, negative crystals of tetrahydrofuran clathrate hydrate and other volatile materials could be made well below the melting temperature.

Finally, all these crystals should undergo either regelation or material transport[10], that is, at the melting temperature should freeze together when touched together, should pass a weighted wire, and should make good snowballs.

We thank Dr D. D. Klug for useful discussions.

Received 11 January; accepted 18 February 1987.

1. Tyndall, J. *Proc. R. Soc. A.* **9**, 76–80 (1858).
2. Davidson, D. W. in *Water a Comprehensive Treatise* Vol. 2 (ed. Franks, F.) 115–234 (Plenum, New York, 1973).
3. Gough, S. R. & Davidson, D. W. *Can. J. Chem.* **49**, 2691–2699 (1971).
4. Kass, M. & Magun, S. *Z. Krist.* **116**, 354–370 (1961).
5. Hawkins, R. E. & Davidson, D. W. *J. phys. Chem.* **70**, 1889–1894 (1966).
6. Wickert, J. N., Tamplin, W. S. & Shank, R. L. *Chem. Engng Progr. Symp. Ser. 2* **48**, 92–96 (1952).
7. Tamman, G. & Krige, G. R. J. *Z. anorg. allgem. Chem.* **146**, 179–195 (1925).
8. Müller-Krumthar, H. in *Physics of Ice* (eds Riel, N., Bullemer, B. & Engelhardt, H.) 132 (Plenum, New York, 1969).
9. Adams, J. M. & Lewis, W. *Rev. Sci. Instrum.* **5**, 400–402 (1934).
10. Knight, C. A. & Knight, N. C. *Science* **150**, 1819–1821 (1965).
11. Hobbs, P. V. *Ice Physics* Ch. 6. (Clarendon, Oxford, 1974).

Forces between surfaces bearing terminally anchored polymer chains in good solvents

Hillary J. Taunton, Chris Toprakcioglu, Lewis J. Fetters* & Jacob Klein†‡

Cavendish Laboratory, Madingley Road, Cambridge, CB3 0HE, UK
* Exxon Research and Engineering Corporation, Annandale, New Jersey 08801, USA
† Polymer Research Department, Weizmann Institute of Science, Rehovot 76100, Israel

The adsorption of high polymers modifies the short-range forces between surfaces in liquid media and is widely used to stabilize or flocculate colloidal dispersions[1]. Previous studies have shown that low surface-coverage by the polymer leads to long-range bridging attraction between the surfaces[2], whereas repulsion sets in at high adsorbance in good solvents[3,4]. In addition, marked hysteresis has been observed for both adsorbed homopolymers and co-polymers on approach and rapid separation of the surfaces[3–5]. Here we report the direct measurement of forces between terminally anchored, non-adsorbing polymer chains (polystyrene) in good solvents (toluene and xylene). The polymer layers are found to extend some $6R_g$ (where R_g is the unperturbed radius of gyration of the polymer) out from each surface, substantially further out than adsorbing homopolymers. Monotonically increasing repulsive forces are observed as the surfaces approach each other and there is no evidence of bridging attraction at low-surface coverage. In addition we find that the force law is reproducible and independent of compression/decompression rates, in marked contrast with adsorbed homopolymers.

‡ To whom correspondence should be addressed.

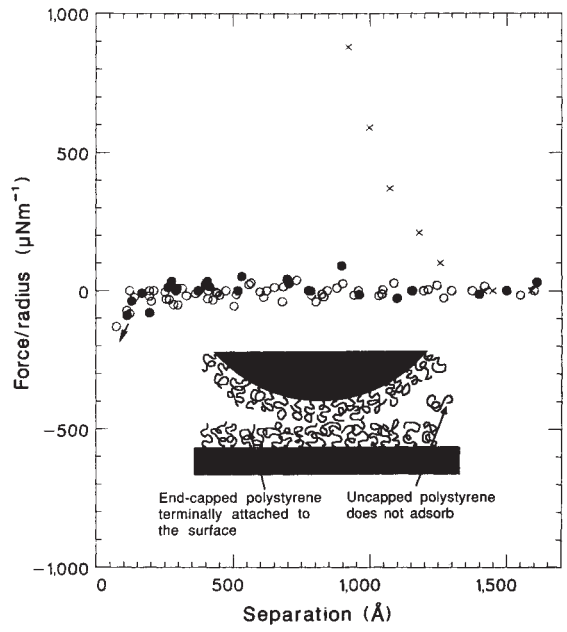

Fig. 1 Force-distance profiles for mica and polystyrene in xylene/toluene, measured using the force-balance technique. ●, Forces $F(D)$ between curved mica surfaces, radius of curvature R, in pure xylene (the result in toluene is identical). ○, Forces $F(D)$ after addition of unfunctionalized polystyrene and 12 h equilibration. The arrow is indicative of a jump into an adhesive contact, and occurs both before and after the addition of the polymer solution; crosses: 2 h after addition of end-capped polystyrene. The data are plotted as $F(D)/R$, which gives the corresponding interaction energy per unit area between flat plates distance D apart, in the Derjaguin approximation[16].

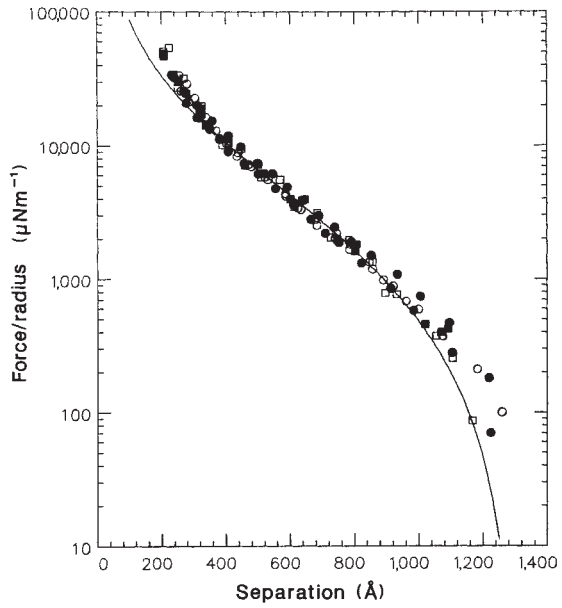

Fig. 2 Forces following saturation adsorption of PS-X. The squares and circles represent the results of two separate experiments. Solid symbols show the forces measured on compression of the adsorbed layers, and open symbols the corresponding forces on rapid decompression. Several compression/decompression cycles are shown. The solid line is the predicted energy $U(D)$ per unit area between flat plates a distance D apart, where $U(D) = \int_{2L}^{D} F(D')\,dD'$ and $F(D)$ is given by equation 1 in the text. The value of L used in 650 Å, as measured from Fig. 1.

The forces F(D) between atomically smooth, crossed cylinders of mica, radius of curvature $R(\sim 1$ cm) and distance D apart, were measured using the force-balance technique[6,7]. The method also measures the refractive index of the medium separating the surfaces, and thus permits an estimate of the amount of adsorbed species.

The polymer/solvent systems used were polystyrene in toluene and polystyrene in xylene, both being good solvents for the polymer. The molecular characteristics of the polymer are given in Table 1. The mica–mica interaction in polymer-free solvent was in all cases measured as a control before the addition of polymer, and is shown in Fig. 1. The absence of any long range interaction and the jump into contact from about 100 Å (attributed to water-bridging in the undried solvent) are similar to previous studies[4]. Linear polystyrene (PS) was then added to the solvent to a concentration of 10^{-4} g ml^{-1} and allowed to equilibrate with the mica surface for 12 ± 1 h. Previous investigations[4] have indicated that polystyrene does not adsorb on to mica from undried toluene. The present study confirms this in both toluene and xylene, as the intersurface forces following equilibration with polystyrene are essentially unchanged from the pure solvent case (Fig. 1). But on replacement of the PS solution with a solution of the same concentration of end-functionalized polystyrene, PS-X (Table 1), where X is the zwitterion group $-N^{+}(CH_3)_2(CH_2)_3SO_3^{-}$, adsorption of the PS-X on to the mica was seen within 1 h as evidenced by the appearance of a repulsion in place of the marked attraction observed both with pure solvent and with the unfunctionalized PS. As the only difference between the two polymer chains is the presence of the zwitterion group in the end-functionalized polystyrene PS-X, this shows unambiguously that the PS-X chains are anchored to each mica surface by the highly polar X moiety, as indicated in Fig. 1.

Figure 2 shows the force-distance profile following saturation adsorption at different rates of approach and separation of the surfaces. The onset of repulsion is first detected at a separation of $1,250 \pm 70$ Å, indicating that the effective extension of the end-anchored polymer layers is ~650 Å (that is $\sim 6R_g$) from each surface. This highly extended configuration contrasts with measurements for adsorbed polymers in good solvents, where the extension is $\sim 3R_g$ from each surface[2–4]. Within the scatter, the profiles in Fig. 2 are independent of compression and decompression rates, again in contrast with adsorbed polymers, where marked hysteresis is a characteristic feature[2–4]. The large non-equilibrium relaxation effects observed with adsorbed chains in good solvents have been attributed to more monomers being forced on to the surface under compression[4]. In a system where the polymer does not adsorb but is only terminally attached, as in our study, no such effects would be expected.

Our results differ considerably from an earlier study of forces between surfaces in a solution of the block copolymer polystyrene/poly(vinyl-2-pyridine) (PS/PVP)[5,8], where the data were interpreted in terms of an adsorbing PVP block and a non-adsorbing PS block. Hysteresis was observed[5] at moderate compressions ($>5,000\ \mu$N m^{-1}) for a PS block with relative mass (M_r) of 1.85×10^5 (185 K), whereas repulsion was first noted at surface separations of $\sim 21\ R_g$ (molecular radius of gyration of the PS block). In contrast, no hysteresis could be measured in our experiments, even under the most rapid

Table 1 Molecular characteristics of polymer

Polystyrene sample	M_r	M_r/M_N
PS	1.31×10^5	1.03
PS-X	1.41×10^5	1.02

The relative molecular masses were determined by gel-permeation chromatography. The unfunctionalized polystyrene PS, with microstructure $[CH_2CH(C_6H_5)]_n$, has a butyl and a phenyl group at its respective ends. The end-functionalized polystyrene, PS-X, was prepared using a propane sultone[15]. M_r and M_N are the weight-averaged and number-averaged relative molecular masses respectively.

experimentally accessible compression and decompression rates (<10 min per cycle) and at very high repulsions (50,000 μN m^{-1}). Also, the range of repulsion in our case was very much smaller (~12R_g for a PS block of M_r 145 K). Identical force-distance profiles were measured in toluene and xylene, and the profiles remained stable for a period of up to 8 days. From refractive index measurements, we have determined the surface coverage of PS-X on mica to be 3 ± 0.5 mg m^{-2}. We have not characterized the mica surface itself, but the interactions can be regarded as being due entirely to the end-grafted polymer chains at the separations of interest.

The equilibrium nature of our results permits detailed comparison with molecular theories of interaction between layers of end-anchored polymers[9-12]. Scaling concepts have been used to describe the conformation of terminally adsorbed polymer layers in a good solvent[10]. This approach has been extended[11,12] to obtain a form for the force per unit area, $F(D)$, between parallel flat plates a distance D apart and bearing a high coverage of end-grafted polymer chains

$$F(D) \simeq \frac{kT}{s^3}\left[\left(\frac{2L}{D}\right)^{9/4} - \left(\frac{D}{2L}\right)^{3/4}\right] \quad (1)$$

for $D < 2L$, where k is Boltzmann's constant, T the absolute temperature, L the mean thickness of the end-grafted layer, and s the average distance between the anchor points on the surface. The force arises from two contributions: the first term in the bracket is the osmotic pressure due to the local increase in the polymer concentration between the plates as they are brought together, and the second term is the elastic restoring force.

This equation (corrected for the geometry of our experiment, see legend to Fig. 2) is plotted as the solid line in Fig. 2, shifted by a constant in the y axis, as the scaling argument does not give the numerical pre-factor. There is good agreement between theory and experiment over most of the range; the discrepancy at small separations may be due to the inapplicability of the scaling theory and volume exclusion effects at the high polymer concentrations in the intersurface gap.

The scaling model also gives an estimate of the layer thickness in a good solvent,

$$L = s\left[\frac{R_F}{s}\right]^{5/3} \quad (2)$$

where R_F is the end-to-end dimension of the polymer in a good solvent. We can evaluate the mean distance between anchor points, s, from the surface coverage estimated from our refractive index data, and R_F from intrinsic viscosity data[13,14]: we find that equation 2 predicts L to be 740 ± 50 Å, which compares closely with our measured value of 650 ± 50 Å. Experiments varying both s and R_F (by changing M_r) are in progress.

This study shows directly that the interaction between layers of end-grafted, non-adsorbing polymer molecules in good solvent conditions is monotonically repulsive, non-hysteretic and considerably longer-ranged than for the corresponding adsorbing chains. The quantitative agreement of our results with the prediction of scaling models suggests that a scaling approach could be of considerable value in understanding the interactions between surfaces bearing terminally anchored polymer layers.

An SERC case studentship with Unilever (H.J.T.) and the partial support of the Israeli Academy Research Division (J.K.) are gratefully acknowledged. J.K. is the incumbent of the Herman Mark Chair of Polymer Physics. The authors thank T. M. Nicholson, and R. Yerushalmi-Rozen, and Prof. M. Tirrell and Prof. D. Tabor for comments on the manuscript.

Received 4 September 1987; accepted 5 February 1988.

1. Napper, D. H. *Polymeric Stabilisation of Colloidal Dispersions* (Academic, London, 1983).
2. Klein, J. & Luckham, P. F. *Nature* **308**, 836-837 (1984).
3. Klein, J. & Luckham, P. F. *Nature* **300**, 429-431 (1982).
4. Luckham, P. F. & Klein, J. *Macromolecules* **18**, 721-728 (1985).
5. Hadziioannou, G., Patel, S., Granick, S. & Tirrell, M. *J. Am. chem. Soc.* **108**, 2869-2876 (1986).
6. Israelachvili, J. N. & Adams, G. E. *J. chem. Soc. Faraday I* **74**, 975-999 (1978).
7. Klein, J. *J. chem. Soc. Faraday I* **79**, 99-118 (1983).
8. Tirrell, M., Patel, S. & Hadziioanou, G. *Proc. natn. Acad. Sci. U.S.A.* **84**, 4725-4728 (1987).
9. Dolan, A. K. & Edwards, S. F. *Proc. R. Soc.* A **343**, 427-442 (1975).
10. Alexander, S. *J. Phys. Paris* **38**, 983-987 (1987).
11. De Gennes, P. G. *C. hebd. Séanc. Sci.* **300**, 839-843 (1985).
12. De Gennes, P. G. *Scaling Concepts in Polymer Physics* (Cornell University Press, Ithaca (1979).
13. Roovers, J. E. & Bywater, S. *Macromolecules* **5**, 385-390 (1972).
14. Einaga, Y., Miyaki, Y. & Fujita, M. *J. Polym. Sci.* **17**, 2103-2109 (1979).
15. Davidson, N. S., Fetters, L. J., Funk, W. H., Graessley, W. W. & Hadjichristidis, N. *Macromolecules* (in the press).
16. Derjaguin, B. V. *Kolloid. Zh.* **69**, 155-164 (1934).

Long-term variation in seawater composition at the base of the thermocline

Francis J. Sansone, S. V. Smith*, James M. Price, Ted W. Walsh*, Thomas H. Daniel† & Christine C. Andrews

Department of Oceanography and Hawaii Institute of Geophysics and * Hawaii Institute of Marine Biology, University of Hawaii, 1000 Pope Road, Honolulu, Hawaii 96822, USA
† Natural Energy Laboratory of Hawaii, P.O. Box 1749, Kailua-Kona, Hawaii 96745, USA

Measurements of the chemical composition of seawater over a time scale of years at a fixed point in the ocean below the main thermocline have not been previously reported because of navigational limitations, ship and hydrowire instability, and, to a large extent, cost. The deep-water pipeline at the Natural Energy Laboratory of Hawaii at Keahole Point (Fig. 1*a*) provides a unique opportunity to address the question of time-varying water composition at a fixed site in the ocean below the mixed layer. In this study we examine the composition of sub-thermocline seawater through weekly sampling (surface-water data are also available, but are not discussed here). The mean deep-water composition obtained over about five years is representative of regional mean-water composition, and significant variation in water composition is observed on time scales exceeding one year. This unexpected long-term variation probably represents cyclic displacement of deep water masses in response to variation in the regional ocean circulation.

The most detailed long-term record of seawater chemistry known to the authors is the Panulirus Station 'S' data set, collected by the Bermuda Biological Station from south of Bermuda at monthly intervals from 1952 to the present[1]. Although this record has proved valuable in many oceanographic studies, horizontal sampling locations are known only within kilometres, and depths are inferred from reversing thermometer data. In contrast, the National Energy Laboratory of Hawaii (NELH) has pumped sub-thermocline water virtually without interruption since mid-1982 through a pipe with an intake depth of 586 m, as part of an ocean-thermal energy conversion (OTEC) and aquaculture test facility (Fig. 1*b*). The intake of the pipe is located 25 ± 5 m above the rocky sea floor, and is 1,700 m offshore. The composition of this water has been measured roughly every week over that period, and additional shorter-term experiments have examined water composition over periods ranging from hours to 50 days. The present paper uses data from weekly samples collected between August 1982 and December 1987.

This paper addresses two primary questions. First, does the water composition obtained from the pumped seawater reflect the mean water composition in the region of the Hawaiian Islands? We will demonstrate that Keahole mean water composition closely matches the composition of open-ocean water in the Hawaiian region. This result will allow examination of the